AMERICAN SCIENTIFIC PUBLISHERS

Journal of Nanofluids
Vol. 8, pp. 1–18, 2019
(www.aspbs.com/jon)

ARTICLE

Heat Transfer During Quenching in Graphene and Multiwall Carbon Nanotubes Nanofluids Under Agitated Quench Conditions

U. Vignesh Nayak and K. Narayan Prabhu*

Department of Metallurgical and Materials Engineering, National Institute of Technology Karnataka, Surathkal, Srinivasnagar, Mangalore 575025, India

Distilled water and aqueous graphene nanofluids of concentrations 0.01, 0.1 and 0.3 vol.% and MWCNT nanofluids of 0.0003, 0.003 and 0.3 vol.% were used as quench media and studied their heat transfer characteristics. ISO 9950 inconel metal probe was used to obtain the thermal history during quenching. The quenching media were agitated in a standard Tensi agitation system at impeller speeds of 0, 500, 1000 and 1500 rpms. Spatio temporal heat flux was obtained by inverse heat conduction method. The rewetting characteristics of nanofluids were obtained and compared with distilled water. Heat transfer analysis showed highest mean heat flux of 3.23 MW/m^2 and fastest heat extraction with 0.1 vol.% graphene nanofluid.

KEYWORDS: Quenching, Agitation, Graphene Nanofluids, MWCNT Nanofluids, Spatiotemporal Heat Flux.

1. INTRODUCTION

Quench hardening is an industrial process used to strengthen metal alloys. Hardening of steels is done by heating it above the austenitization temperature (generally above 860 °C), followed by rapidly cooling in a heat transfer medium. Generally, liquid quenching media are preferred as they provide faster and higher heat transfer capabilities compared to gaseous and solid media. In the early period of development of quenching technology, water was used to quench harden steel. This was because of its ease of availability and low cost. However, quenching with water was found to be disadvantageous as water does not wet the surface of the metal uniformly. Moreover, the quench severity of water is high and is not suitable for quench hardening high alloyed steels and steels having intricate shapes. Efforts directed towards minimizing/eliminating these drawbacks by increasing the temperature of water caused irregular cooling at low temperatures of 300 to 200 °C in the metal[1] which under increased intensity would cause soft spots, distortion and warping issues.

Nanofluids are heat transfer media obtained by dispersing nano sized particles (1 to 100 nm) of solid materials in base fluids. Nanofluids are formulated from different metallic and nonmetallic materials such as copper, titanium, multiwall carbon nanotubes (MWCNT), silicon carbide and others.[2] In quenching heat treatment, the performance of the quenchant is measured by its ability to extract heat from the hot metal surface. At low concentrations of nanoparticles, the cooling curves measured for water and nanofluids showed no increase in cooling with nanofluids. Repetitive quenching experiments with water based alumina, silica and diamond nanoparticles[3] showed the deposition of particles on the quench probe surface. The effect of deposition was to increase the cooling rate during quenching and was also observed in the works of Ref. [4]. Zupan et al.[5] reported increase in the peak heat transfer coefficient in nanofluids relative to their base fluids (water and PAG solution, 5, 10 and 20 Vol.%) with the addition of 0.2 g/l of nanoparticles under unagitated quench condition. These studies highlight the shortening of the film boiling stage indicating early wetting of the cooling metal surface. Babu and Kumar[6] used CNT nanofluids for quenching 304L SS probe and showed higher peak heat flux at bath temperature of 40 °C. They attributed the increase in peak heat flux was caused due to the increase in random motion of the particles in water. Quenching of fresh probe in water-clay nanofluids of various concentrations lowered the peak heat flux compared to quenching in water.[7] These outcomes indicate the importance of selecting the material type while formulating the nanoquenchant. Copper nanofluid quench medium of concentration 2.6 mg/L prepared by laser ablation method was studied for its heat transfer characteristics and compared

*Author to whom correspondence should be addressed.
Email: prabhukn_2002@yahoo.co.in
Received: 13 July 2018
Accepted: 1 November 2018

Table I. Details of quench media.

Sl no.	Nanoparticles	Size	Concentrations (vol.%)	Mode of preparation	Source
1	Distilled water				Prepared in the laboratory
2	Multi wall carbon nanotube (MWCNT)	Upto 500 nm	0.0003 0.003 0.03	Mechanical mixing using a hand held stirrer	Timesnano Co., Chengdu, China
4	Graphene	1 to 5 nm thick	0.01 0.1 0.3	Ultrasonication at 30 kHz for 30 minutes	Reinste Nano Ventures Pvt. Ltd.

with deionised water. Results obtained during quenching under agitation rates of 0, 390, 850 and 1170 rpm showed increased cooling rates for the nanofluid compared to water at 0 rpm, lower cooling rates at 390 rpm and similar cooling rates at 850 and 1170 rpms.[8] Chemically

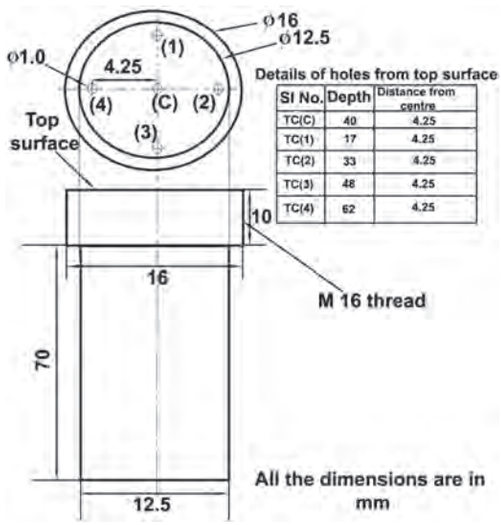

Fig. 1. Design of the inconel quench probe with holes for inserting thermocouples.

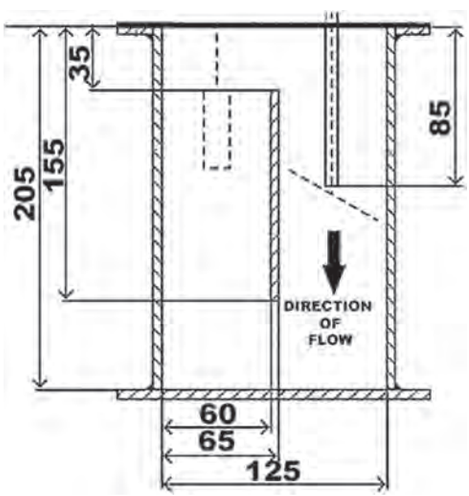

Fig. 2. Tensi agitator.

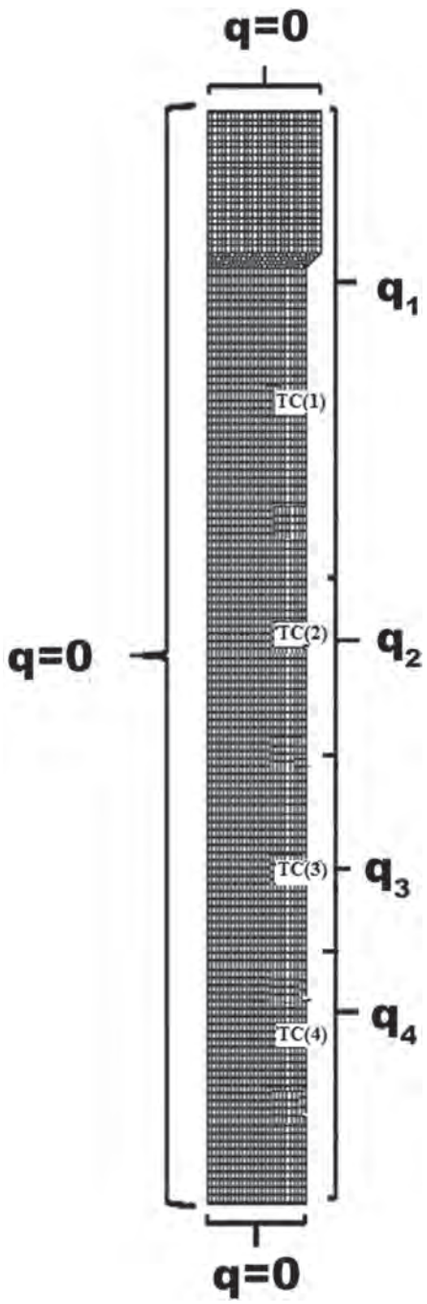

Fig. 3. Axisymmetric meshed model of the quench probe.

treated CNT nanofluid of 0.5 wt.% concentration was studied for its heat transfer capability at impeller agitation rates of 1000 and 1600 rpms using a vane type mechanical stirrer by Babu and Kumar.[6] They used 2L of quench medium. Their results showed a decrease of about 30% and 22% in the peak heat flux and reduced heat extraction ability of the nanofluid when quenching was carried out at 1600 and 1000 rpm impeller rates respectively.

The objectives of the present investigation are (i) To assess the wetting behaviour of nanofluids as it influences the uniformity with which heat is removed. (ii) To assess the heat removal ability of aqueous nanofluids under agitation and to compare them with distilled water quench medium so as to obtain a quench medium that would lead to improved mechanical properties in steel during quenching. In the present work, aqueous graphene and MWCNT of various concentrations were prepared by the two-step method. Thermal conductivity, viscosity, density and surface tension of nanofluids were measured. The spreading behaviour of nanofluid droplet on an inconel substrate was studied. Quenching experiments under agitated quench conditions were carried out to assess their heat extraction ability and were compared with distilled water. The interfacial spatiotemporal heat flux during quenching was computed by inverse heat conduction method.

2. EXPERIMENTAL DETAILS

2.1. Preparation of Nanofluids

The nanofluids used were prepared by the two-step method. In the two-step method, nanoparticles were procured from commercial suppliers and then dispersed in water. MWCNT procured used was in the paste form while graphene used was in the form of powder. The details of the nanofluid media used and their preparation methods are given in Table I.

2.2. Quench Probe Details

A schematic sketch of quench probes indicating thermocouple locations are given in Figure 1. Cooling

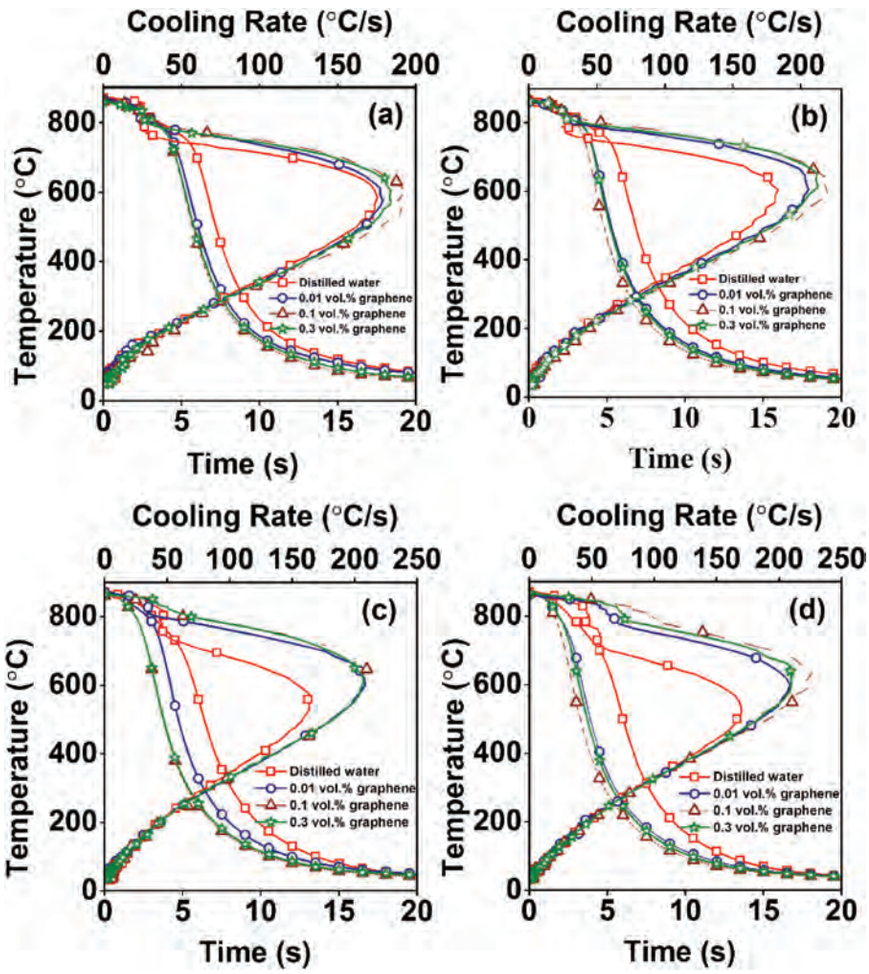

Fig. 4. Cooling curves and cooling rate curves measured at the geometric center of the probe during quenching in graphene nanofluids of various concentrations at impeller agitation rates of (a) still (b) 500 (c) 1000 and (d) 1500 rpms.

characteristics of the quench media were obtained using inconel 600 alloy probe. The probe was machined to dimensions in accordance with the ISO 9950 standard (⌀ 12.5 × 60 mm). The metal probe was drilled at various locations to accommodate ⌀ 1.0 mm *K*-type thermocouples. The drilled holes in the inconel probe had a diameter of 1.0 mm. The inconel probe has a 10 mm screw section to fasten the probe to a connecting pipe. The pipe conceals the entry of liquid medium into the drilled holes and facilitates lateral quenching of the probe.

2.3. Quench Set-Up

The quench experiments under agitation were done using a Tensi agitation system schematically shown in Figure 2. The thermocouple imbedded Inconel probe was heated in an electric furnace to a temperature of 880 °C before transferring it to the Tensiagitation system. The cold junction of the thermocouples was connected to data acquisition system (DAQ, NI 9213) via *K*-type compensating cables. DAQ was interfaced with a computer to record the thermal history during quenching. The Tensi system was made up of plexiglass quench tank of dimensions shown in the figure and contained 1.5 lts. of the quench medium. The quench medium was agitated using a four-bladed propeller. Three propeller speeds of 0, 500, 1000 and 1500 rpm were provided during the lateral quench experiments. During the quenching process, the system was placed beside the furnace and the probe was manually transferred from the electric furnace to the Tensi quench tank. The surface temperature of the probe as measured by the near surface sensors dropped by about 10 to 15 °C during the transfer. The hot probe was quenched in the liquid medium when one of the near surface sensor reached a temperature of about 860 °C. In all the experiments, the impeller was operated prior to the immersion of the hot probe and the temperature of the quenching medium at the start of the quenching process was in the range of 28 ± 3 °C. The thermal data was recorded at intervals of 0.1 s and the probe was cleaned with water and acetone after each cycle.

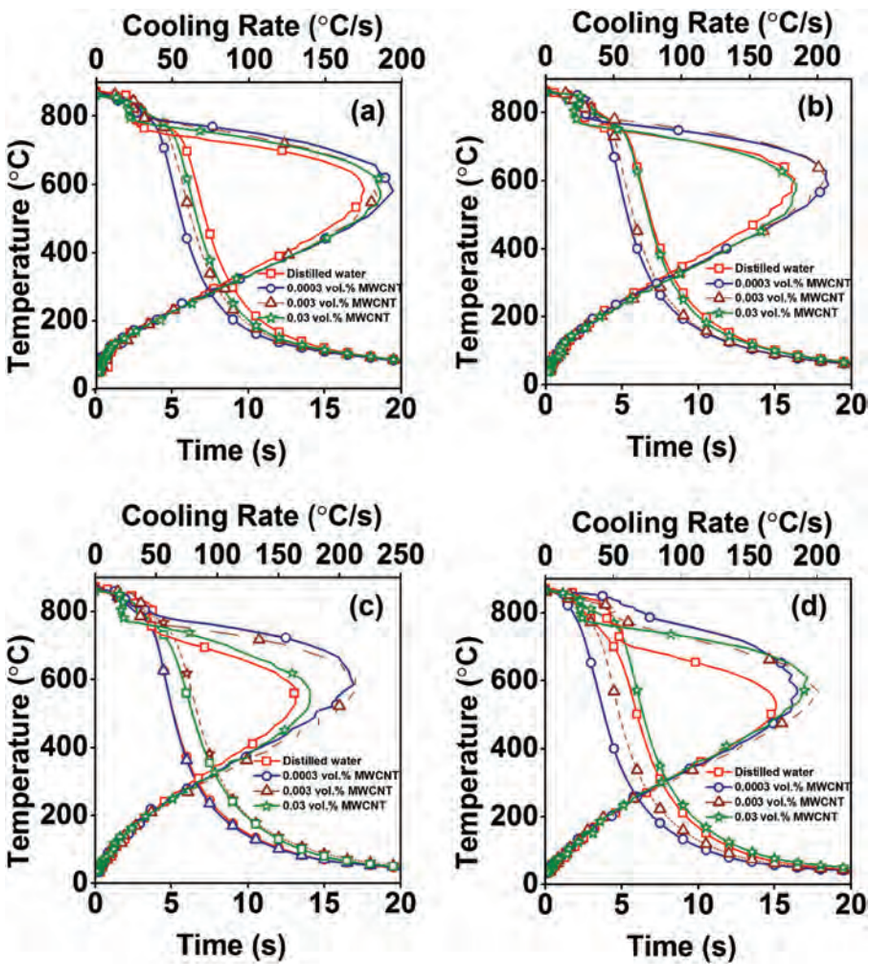

Fig. 5. Cooling curves and cooling rate curves measured at the geometric center of the probe during quenching in MWCNT nanofluids of various concentrations at impeller agitation rates of (a) still (b) 500 (c) 1000 and (d) 1500 rpms.

2.4. Measurements of Viscosity, Thermal Conductivity and Density

Viscosity of the quench medium was measured using a programmable rheometer (Brookfield LDV-IIIU, Brook field Engineering Laboratories, Inc., USA). The viscosity of water and nanofluids were measured using ultra low adapter (ULA) spindle. The spindle was immersed into specially designed sample chamber containing 16 ml of test liquid was used to measure the viscosity.

Thermal conductivity of nanofluids was measured using KD2-Pro device with KS-1 sensor. To make measurements, the sensor was dipped in a 100 ml beaker containing 90 ml of nanofluid medium. Density of quench media was measured by the weight displacement method. For this purpose, a 50 ml specific gravity bottle was used.

2.5. Measurement of Contact Angle and Surface Tension

Wetting of the liquid quench medium on the probe surface has been reported to influence the cooling process. The contact angle of a droplet and its spreading behaviour was studied using KRUSS drop shape analyser (DSA 100S). A 1 ml surgical syringe fitted with a needle having 0.5 mm diameter was used to dispense a droplet of quench medium on the substrate. The amount of droplet dispensed was controlled using a precision pump. The spreading phenomenon of the droplet on the metal substrate was recorded by a high-speed camera operated at 26 fps and the images were analysed in KRUSS Advance software. Elliptical curve fitting method inbuilt in the software was used to measure the contact angle of the dispensed drop. For measuring the surface tension, the syringe was fitted with a needle of 1.83 mm in diameter. To make measurements, a pendant of the quench medium was formed and suspended from the tip of the needle. Density and viscosity of the liquid used were provided as inputs to the Advance software to obtain the surface tension. The ambient temperature during experiments was maintained at 26 °C. The captured images were analysed in the Advance software to measure the dynamic contact angle.

2.6. Interfacial Heat Flux Transients

The spatiotemporal heat flux transients at the metal/quenchant interface were estimated by inverse heat conduction technique using the near surface thermocouples data. The thermal properties of the inconel probe along with the solution methodology detailed in the Ref. [9] was followed to obtain the interfacial spatiotemporal heat flux. Figure 3 shows 2-D axisymmetric models of various probes. These models were used to estimate the boundary heat flux transients (q). The models were meshed uniformly with 4 node quadrilateral elements. Measured temperature data obtained during quenching experiment was provided as input to these models at nodes corresponding to the locations given in Figure 1. In the inconel probe model, TC(1) represents the temperature readings measured at a depth of 17 mm while TC(2), TC(3) and TC(4) represent the temperatures recorded at depths of 33, 48 and 52 mm respectively and were at 2 mm below the surface. The meshing of model resulted in 3500 elements. The inconel probe model was divided into 4 boundary heat flux segments. The convergence limit in the Gauss-Siedel iterations was set as 10^{-6}.

3. RESULTS AND DISCUSSION

The cooling curve and cooling rate curves obtained at the geometric centre of the probe during quenching in graphene and MWCNT nanofluids of various concentrations are shown in Figures 4 and 5 respectively.

The cooling curves show that quenching of the inconel probe in water and nanofluids proceeded with vapor phase stage in the beginning followed by nucleate boiling and convective cooling. Vapor phase engulfs the probe at the onset of quenching as the temperature of the probe far exceeds the boiling temperature of the liquid quench medium. The heat loss from the probe during this phase is slow because of the insulating nature of the vapor. With continued cooling, vapor phase collapses allowing liquid medium to contact the probe causing increased heat loss.

Table II. Temperature and time at which vapor to nucleate boiling transition at various agitation rates for water and nanofluids.

Agitation rate (rpm)	Quench media	t_{A-B} (s)	T_{A-B} (°C)
Still	Distilled water	4.5	778
	0.01 vol.% graphene	3.3	805
	0.1 vol.% graphene	3	810
	0.3 vol.% graphene	3	808
	0.0003 vol.% MWCNT	2.8	815
	0.003 vol.% MWCNT	3.2	816
	0.03 vol.% MWCNT	3.9	796
500 rpm	Distilled water	3.9	788
	0.01 vol.% graphene	2.9	810
	0.1 vol.% graphene	2.4	825
	0.3 vol.% graphene	3	811
	0.0003 vol.% MWCNT	3.2	789
	0.003 vol.% MWCNT	3.4	802
	0.03 vol.% MWCNT	4.3	774
1000 rpm	Distilled water	3.7	771
	0.01 vol.% graphene	2.5	811
	0.1 vol.% graphene	1.8	813
	0.3 vol.% graphene	1.4	835
	0.0003 vol.% MWCNT	2.7	817
	0.003 vol.% MWCNT	3.3	776
	0.03 vol.% MWCNT	4.1	779
1500 rpm	Distilled water	4.1	724
	0.01 vol.% graphene	2.1	786
	0.1 vol.% graphene	1.4	820
	0.3 vol.% graphene	1.5	828
	0.0003 vol.% MWCNT	2	787
	0.003 vol.% MWCNT	2.6	794
	0.03 vol.% MWCNT	4.1	783

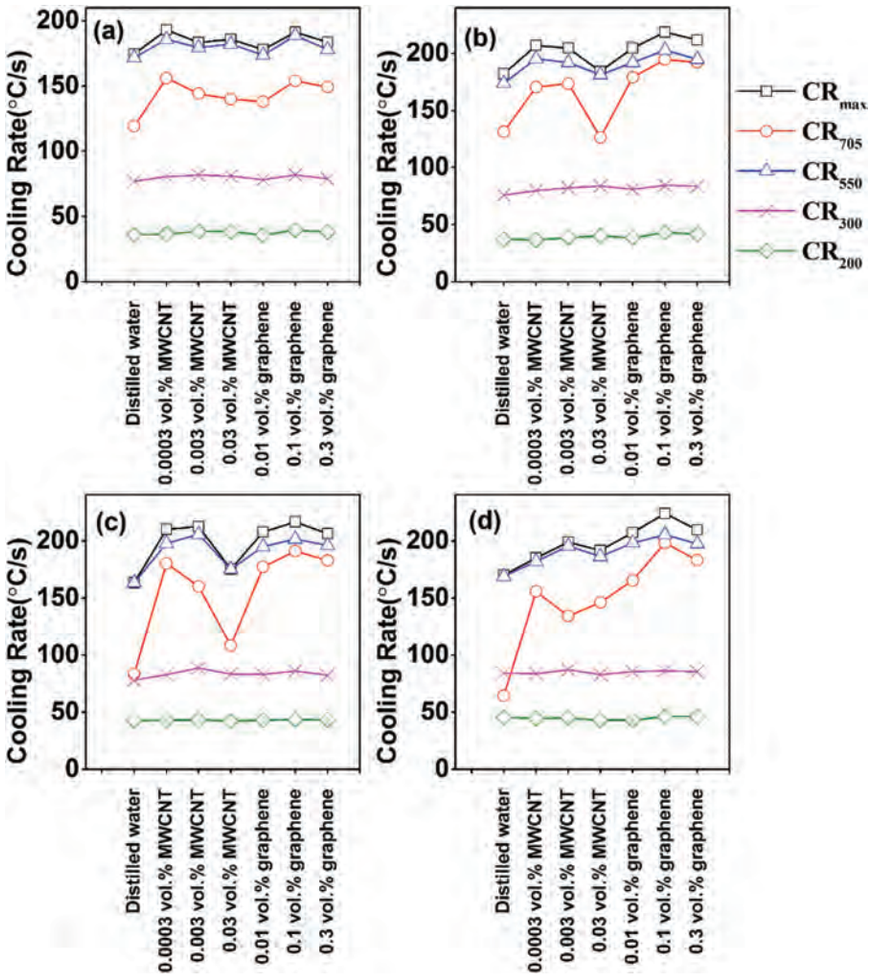

Fig. 6. Cooling rates at critical cooling temperatures for nanofluids under (a) still (b) 500 (c) 1000 and (d) 1500 rpm agitation rates.

The rapid drop in temperature occurs because of the latent heat of vaporization of the quench medium and accompanied by numerous bubbles emanating from the surface of the quenched probe that depart and collapse carrying large quantity of heat with them. This stage of heat loss is followed by the convective cooling stage and occurs as the temperature drops below the boiling point of the medium. The heat loss during convection stage is slower than the nucleate boiling stage with heat being transferred from the probe to the liquid medium until uniform temperature is attained between the probe and the medium. These stages of heat transfer experienced by the probe during quenching are more clearly seen in the cooling rate curves shown in the above figures. The rate of cooling initially is low and slow followed by rapid increase with cooling rate reaching a peak value and then reducing with further progress in cooling until achievement of equilibrium in temperature between the medium and the metal probe. The temperature (T_{A-B}) and time (t_{A-B}) at which the transition from vapor phase to nucleate boiling occurred at the center of the probe during quenching with water and nanofluids under various agitation rates are shown in Table II. The table shows that nanofluids had higher transition temperature and took shorter time to transit from the vapor phase to nucleate boiling stage compared to distilled water. It also shows that with increased agitation rate, higher transition

Table III. Thermo-physical properties of distilled water and nanofluids of graphene and MWCNT of various concentrations.

Quenchants	Viscosity, $\times 10^{-3}$ (Pa·s)	Thermal conductivity (W/mK)	Density (kg/m^3)	Surface tension (mN/m)
Distilled water	1.32 ± 0.01	0.5965 ± 0.06	867.8	72
MWCNT				
0.0003 vol.%	1.29 ± 0.01	0.61425 ± 0.02	868.3	63
0.003 vol.%	1.32 ± 0.01	0.59075 ± 0.05	868.4	48
0.03 vol.%	1.31 ± 0.01	0.59819 ± 0.096	868.6	58
0.01 vol.%	1.31 ± 0.03	0.5389 ± 0.047	868.4	62
Graphene				
0.1 vol.%	1.35 ± 0	0.5908 ± 0.062	868.5	63
0.3 vol.%	1.34 ± 0.02	0.6151 ± 0.078	868.6	63

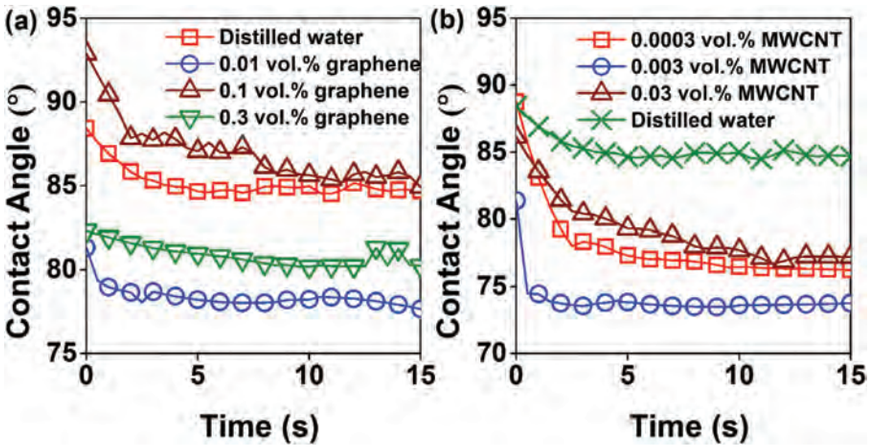

Fig. 7. Contact angle relaxation curves for (a) graphene and (b) MWCNT nanofluids of various concentrations.

temperature and shorter transition time was achieved indicating higher heat transfer with increase in the agitation rate of quench medium.

The critical cooling parameters obtained at the geometric centre of the probe during quenching is shown in Figure 6 and was obtained using the cooling rate data shown in Figures 4 and 5. CR_{max} is the maximum cooling rate obtained during the quenching process and T_{max} refers to the temperature at which the cooling rate becomes maximum. CR_{705} is the cooling rate at 705 °C and it represents the temperature at which austenite in most steels transforms into ferrite and pearlite. CR_{550} is the cooling rate at 550 °C and it is representative of the temperature near the nose of the TTT curve for many steels. CR_{300} and CR_{200} represents the temperatures in the region of martensitic transformation for many steels.

The plots of critical cooling parameters show that higher cooling rates are obtained at the critical temperatures for

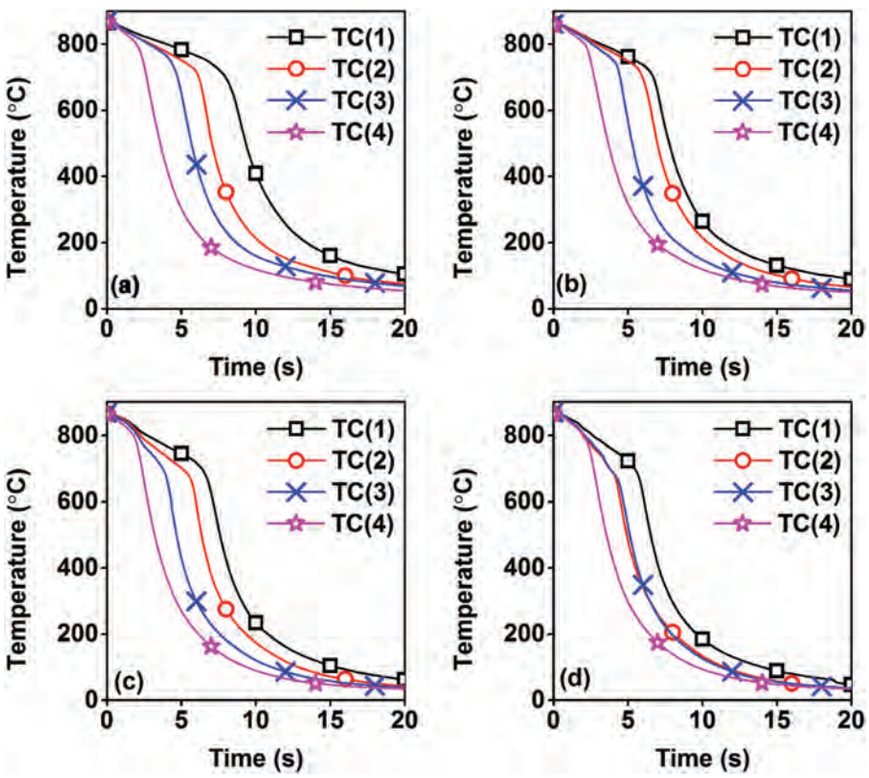

Fig. 8. Cooling curves measured at various axial locations in the probe during quenching in distilled water under (a) still (b) 500 rpm (c) 1000 rpm and (d) 1500 rpm impeller speeds.

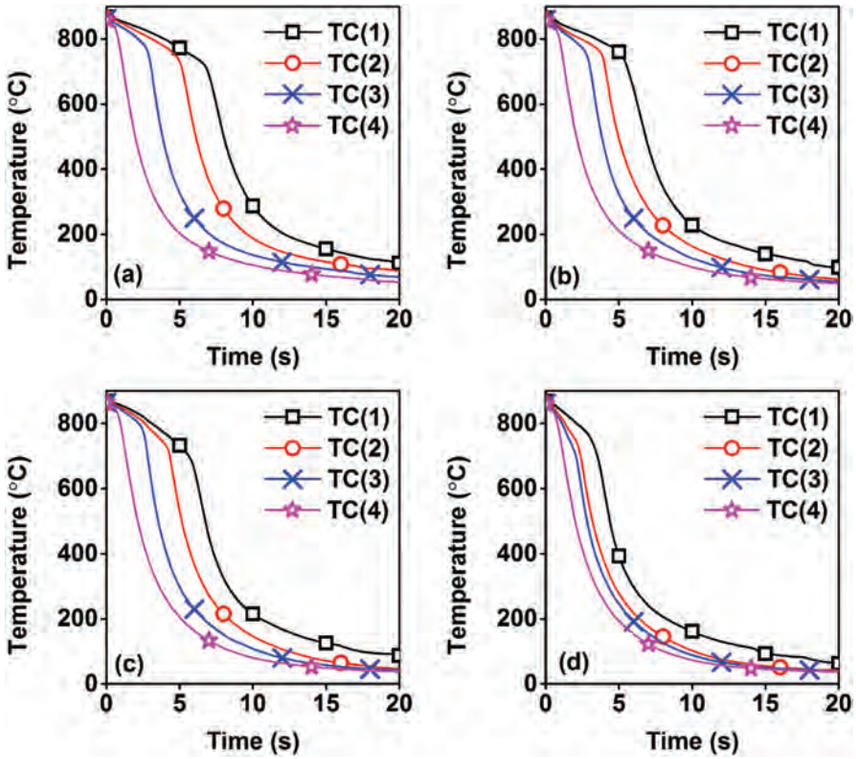

Fig. 9. Cooling curves measured at various axial locations in the probe during quenching in 0.0003 vol.% MWCNT nanofluid under (a) still (b) 500 rpm (c) 1000 rpm and (d) 1500 rpm impeller speeds.

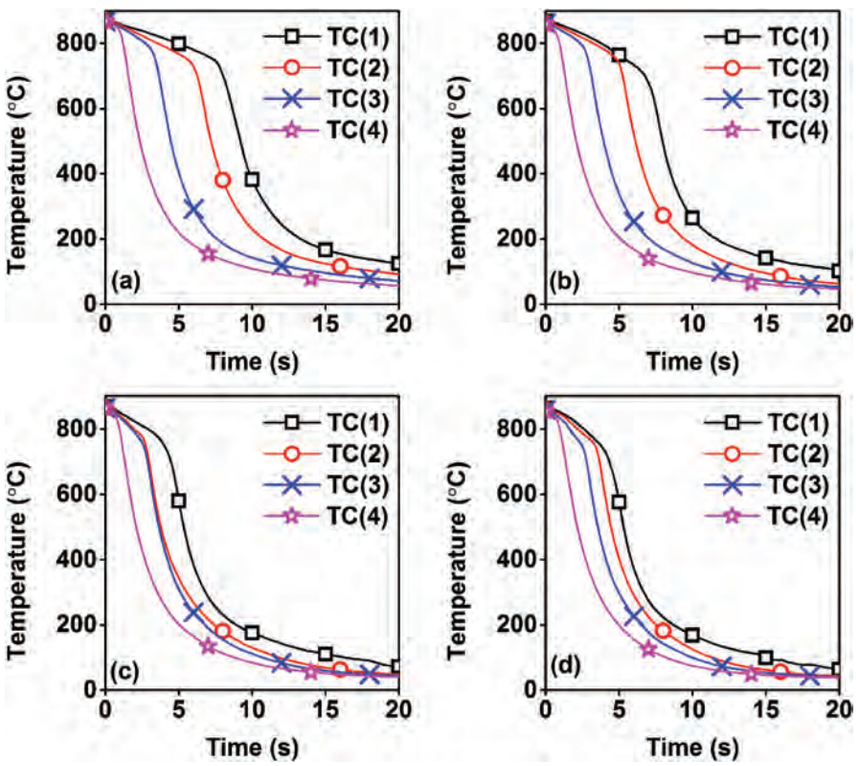

Fig. 10. Cooling curves measured at various axial locations in the probe during quenching in 0.003 vol.% MWCNT nanofluid under (a) still (b) 500 rpm (c) 1000 rpm and (d) 1500 rpm impeller speeds.

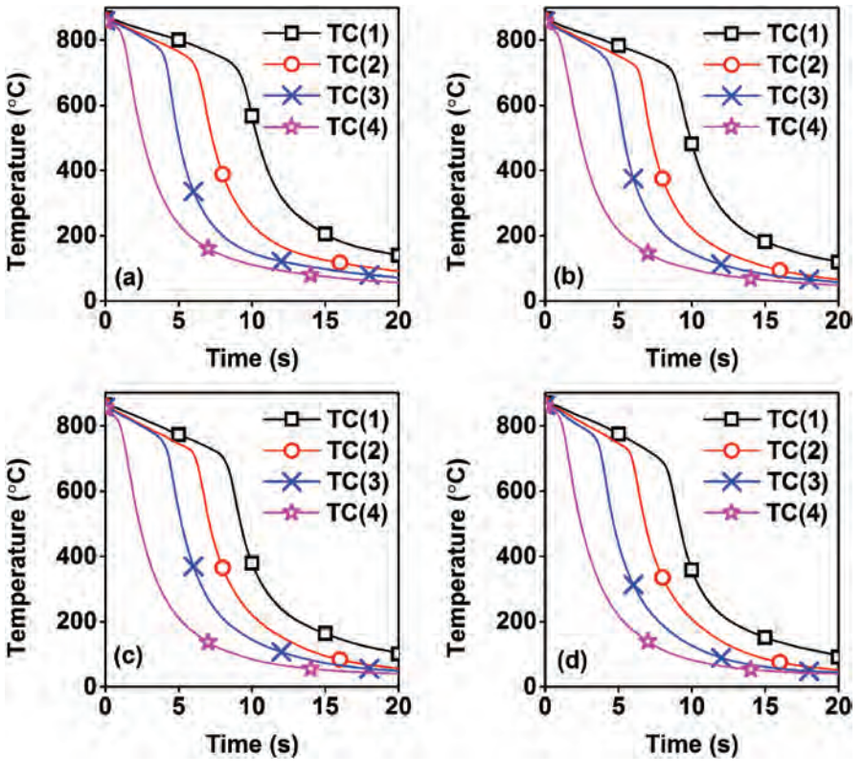

Fig. 11. Cooling curves measured at various axial locations in the probe during quenching in 0.03 vol.% MWCNT nanofluid under (a) still (b) 500 rpm (c) 1000 rpm and (d) 1500 rpm impeller speeds.

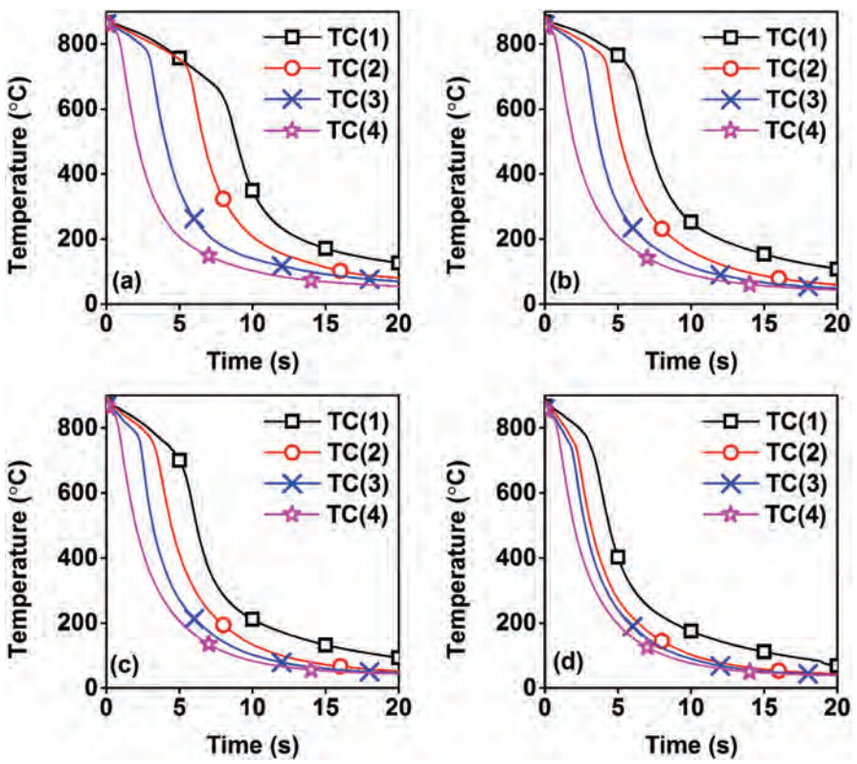

Fig. 12. Cooling curves measured at various axial locations in the probe during quenching in 0.01 vol.% graphene nanofluid under (a) still (b) 500 rpm (c) 1000 rpm and (d) 1500 rpm impeller speeds.

ARTICLE

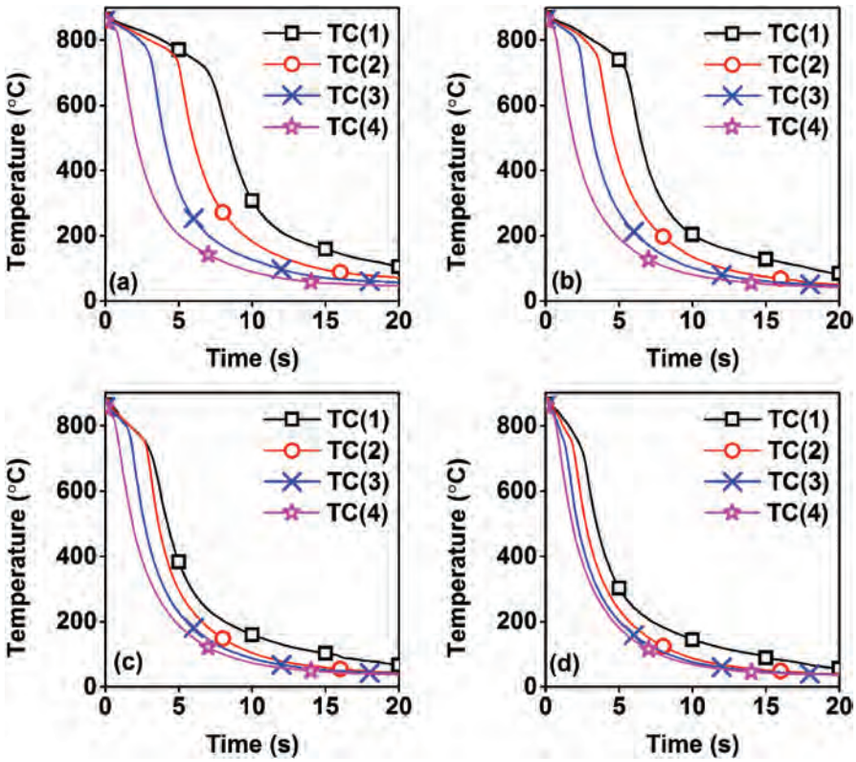

Fig. 13. Cooling curves measured at various axial locations in the probe during quenching in 0.1 vol.% graphene nanofluid under (a) still (b) 500 rpm (c) 1000 rpm and (d) 1500 rpm impeller speeds.

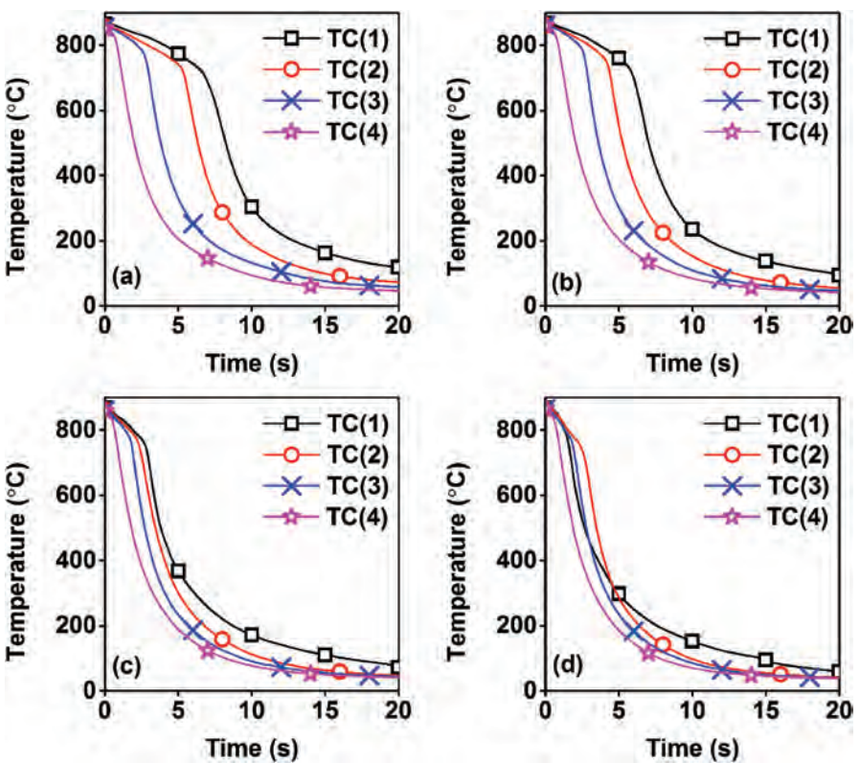

Fig. 14. Cooling curves measured at various axial locations in the probe during quenching in 0.3 vol.% graphene nanofluid under (a) still (b) 500 rpm (c) 1000 rpm and (d) 1500 rpm impeller speeds.

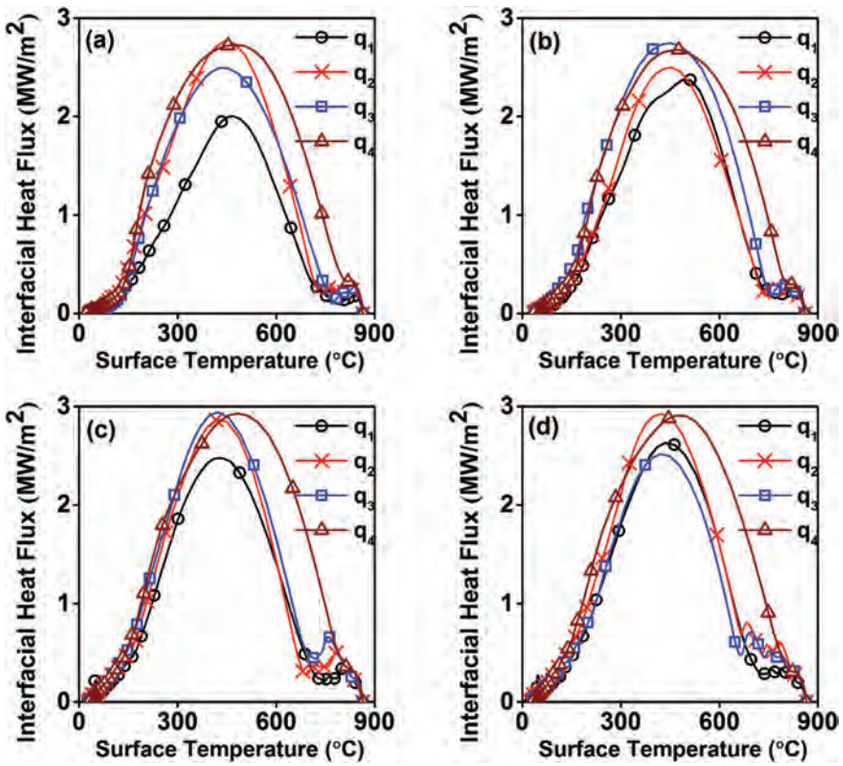

Fig. 15. Heat flux versus surface temperature obtained at various axial locations in the probe during quenching in distilled water under (a) still (b) 500 rpm (c) 1000 rpm and (d) 1500 rpm impeller speeds.

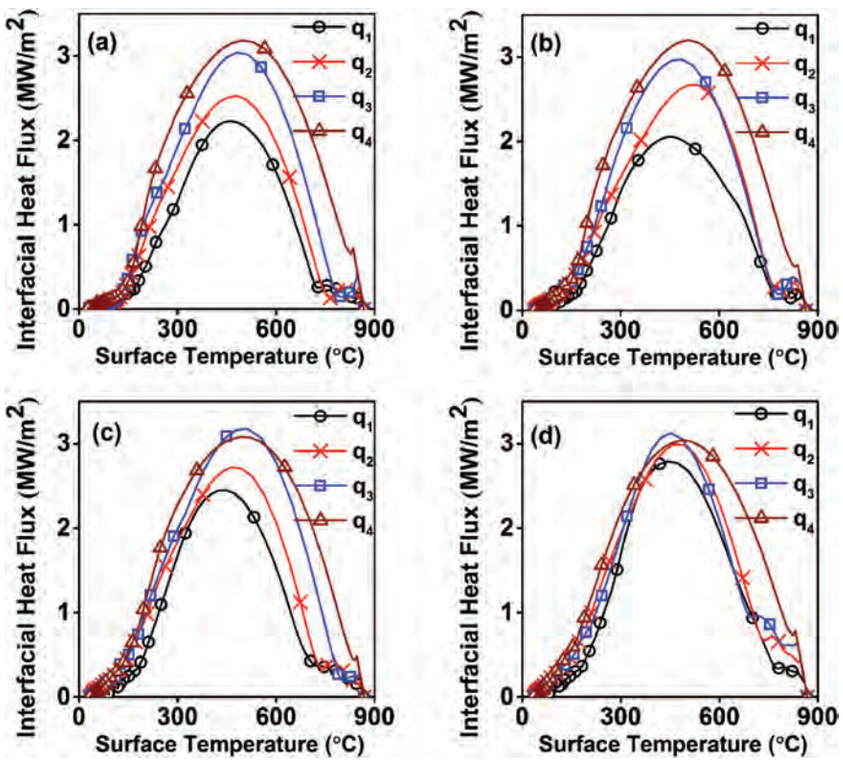

Fig. 16. Heat flux versus surface temperature obtained at various axial locations in the probe during quenching in 0.0003 vol.% MWCNT under (a) still (b) 500 rpm (c) 1000 rpm and (d) 1500 rpm impeller speeds.

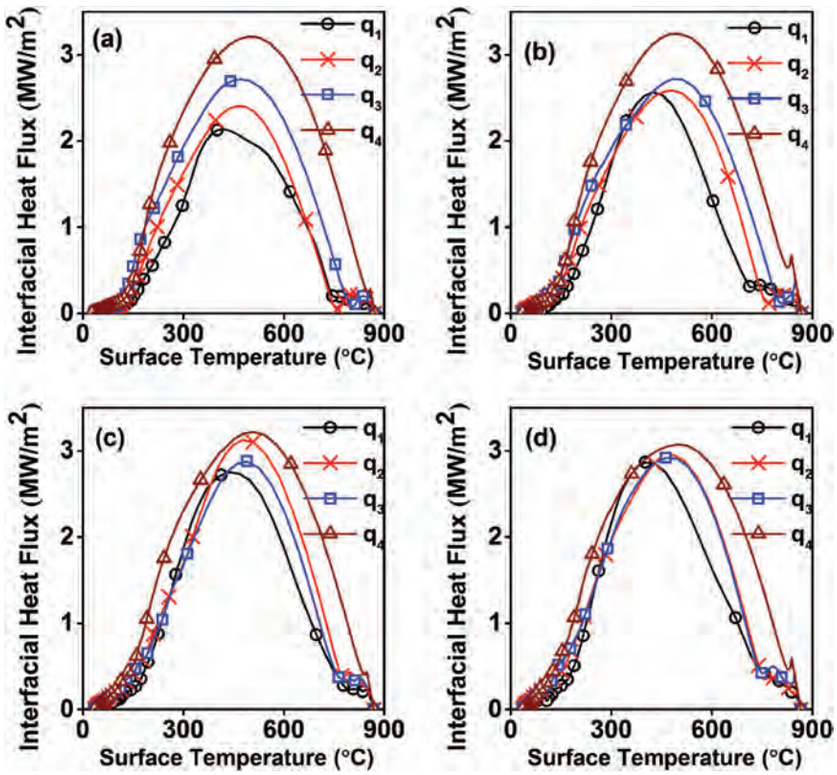

Fig. 17. Heat flux versus surface temperature obtained at various axial locations in the probe during quenching in 0.003 vol.% MWCNT under (a) still (b) 500 rpm (c) 1000 rpm and (d) 1500 rpm impeller speeds.

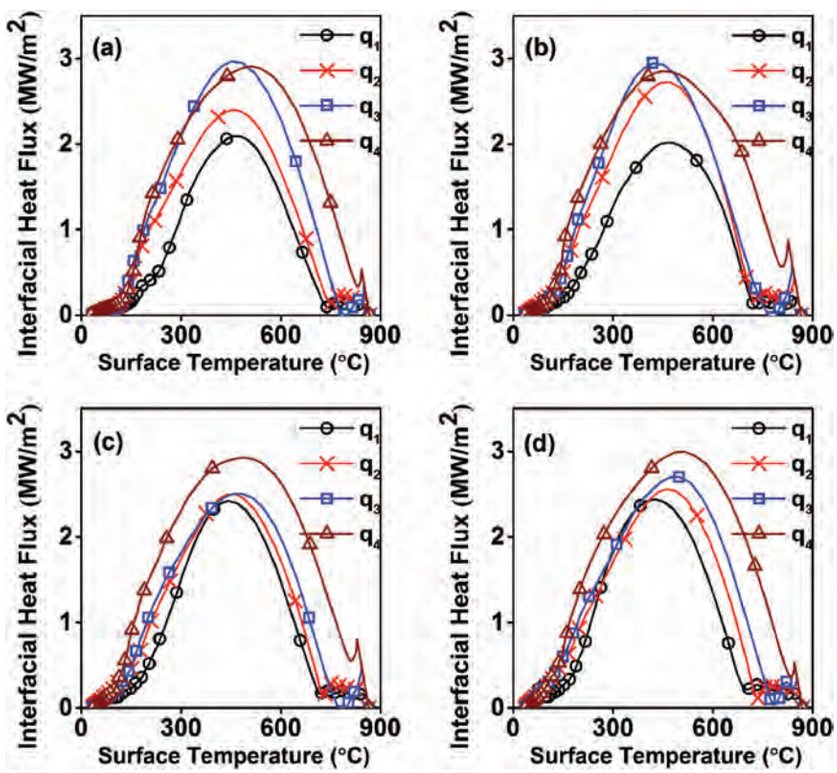

Fig. 18. Heat flux versus surface temperature obtained at various axial locations in the probe during quenching in 0.03 vol.% MWCNT under (a) still (b) 500 rpm (c) 1000 rpm and (d) 1500 rpm impeller speeds.

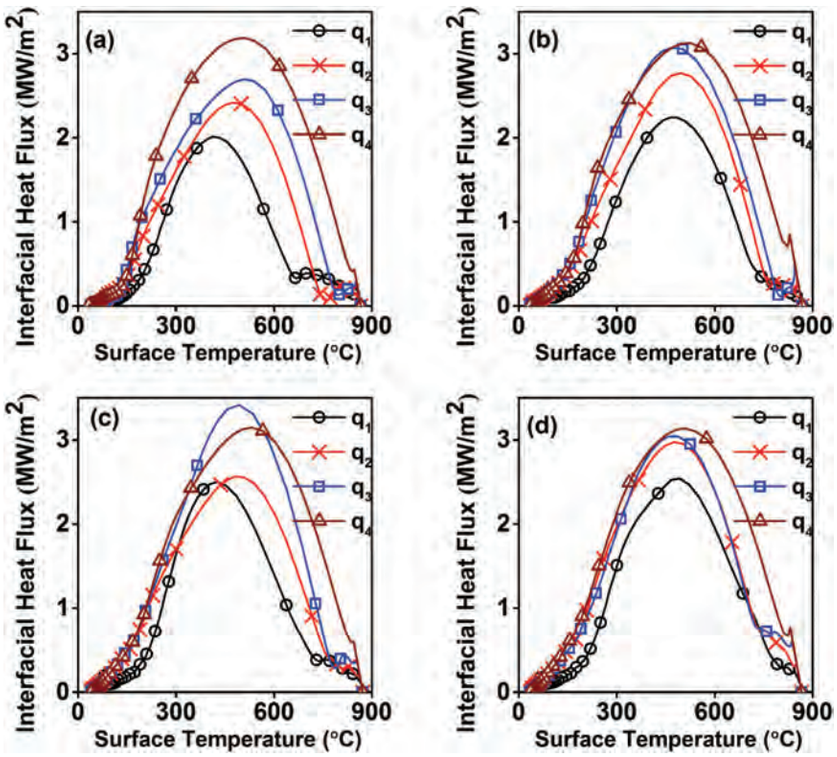

Fig. 19. Heat flux versus surface temperature obtained at various axial locations in the probe during quenching in 0.01 vol.% graphene under (a) still (b) 500 rpm (c) 1000 rpm and (d) 1500 rpm impeller speeds.

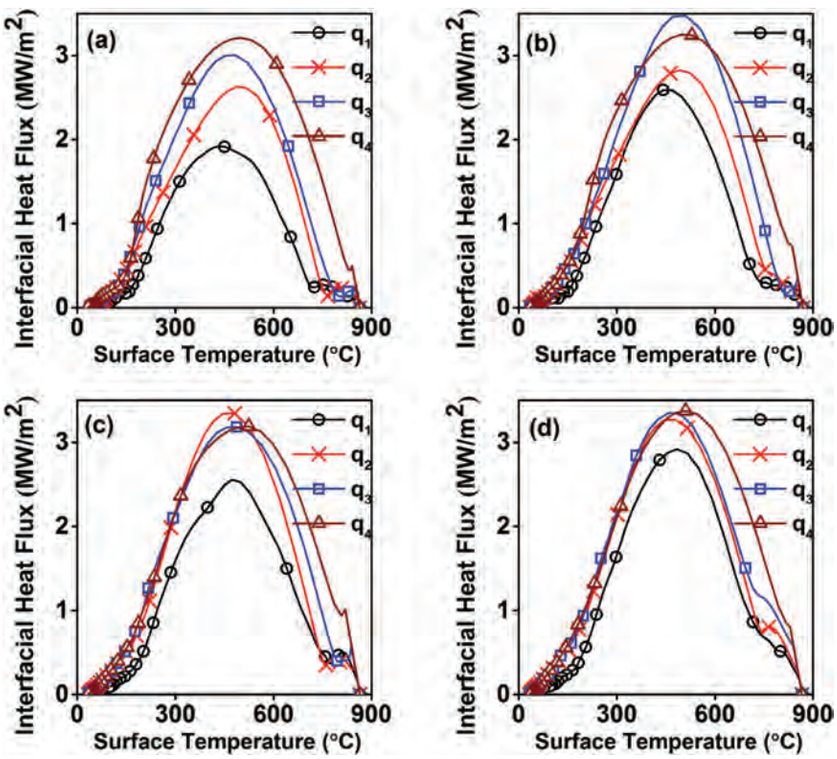

Fig. 20. Heat flux versus surface temperature obtained at various axial locations in the probe during quenching in 0.1 vol.% graphene under (a) still (b) 500 rpm (c) 1000 rpm and (d) 1500 rpm impeller speeds.

ARTICLE

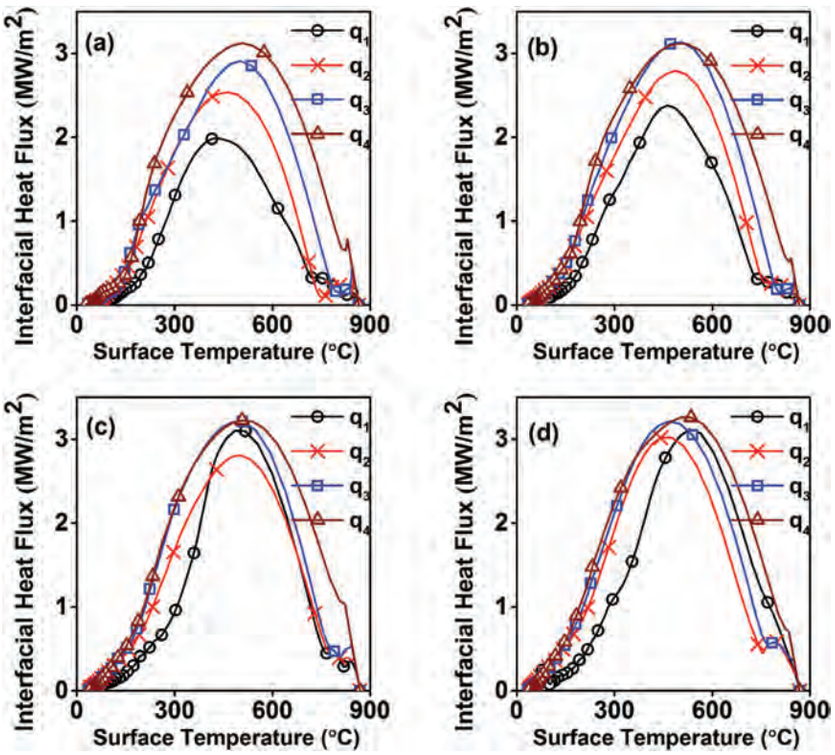

Fig. 21. Heat flux versus surface temperature obtained at various axial locations in the probe during quenching in 0.3 vol.% graphene under (a) still (b) 500 rpm (c) 1000 rpm and (d) 1500 rpm impeller speeds.

Table IV. Peak heat flux values obtained during quenching.

Agitation rate	Quench media	Top half		Bottom half		Average	Standard deviation
		q_1	q_2	q_3	q_4		
					(MW/m^2)		
Still	Distilled water	2.00	2.76	2.50	2.73	2.50	0.35
	0.0003 vol.% MWCNT	2.23	2.52	3.04	3.18	2.74	0.45
	0.003 vol.% MWCNT	2.14	2.40	2.72	3.21	2.62	0.46
	0.03 vol.% MWCNT	2.09	2.40	2.97	2.91	2.59	0.42
	0.01 vol.% graphene	2.01	2.42	2.70	3.19	2.58	0.49
	0.1 vol.% graphene	1.92	2.63	3.01	3.21	2.69	0.57
	0.3 vol.% graphene	1.99	2.54	2.91	3.12	2.64	0.50
500 rpm	Distilled water	2.37	2.50	2.75	2.68	2.58	0.17
	0.0003 vol.% MWCNT	2.06	2.67	2.97	3.20	2.72	0.50
	0.003 vol.% MWCNT	2.56	2.58	2.72	3.24	2.78	0.32
	0.03 vol.% MWCNT	2.02	2.73	2.95	2.86	2.64	0.42
	0.01 vol.% graphene	2.24	2.77	3.07	3.13	2.80	0.41
	0.1 vol.% graphene	2.59	2.83	3.47	3.25	3.04	0.40
	0.3 vol.% graphene	2.38	2.80	3.14	3.12	2.86	0.36
1000 rpm	Distilled water	2.48	2.87	2.94	2.93	2.80	0.22
	0.0003 vol.% MWCNT	2.45	2.72	3.18	3.08	2.86	0.34
	0.003 vol.% MWCNT	2.75	3.13	2.88	3.22	2.99	0.22
	0.03 vol.% MWCNT	2.42	2.50	2.51	2.93	2.59	0.23
	0.01 vol.% graphene	2.50	2.57	3.42	3.15	2.91	0.45
	0.1 vol.% graphene	2.55	3.34	3.18	3.19	3.07	0.35
	0.3 vol.% graphene	3.10	2.81	3.21	3.23	3.09	0.19
1500 rpm	Distilled water	2.63	2.93	2.52	2.91	2.75	0.20
	0.0003 vol.% MWCNT	2.79	2.99	3.13	3.04	2.99	0.14
	0.003 vol.% MWCNT	2.87	2.95	2.92	3.07	2.95	0.09
	0.03 vol.% MWCNT	2.44	2.56	2.70	2.99	2.67	0.24
	0.01 vol.% graphene	2.54	2.97	3.04	3.14	2.92	0.26
	0.1 vol.% graphene	2.92	3.27	3.35	3.38	3.23	0.21
	0.3 vol.% graphene	3.12	3.02	3.21	3.26	3.15	0.11

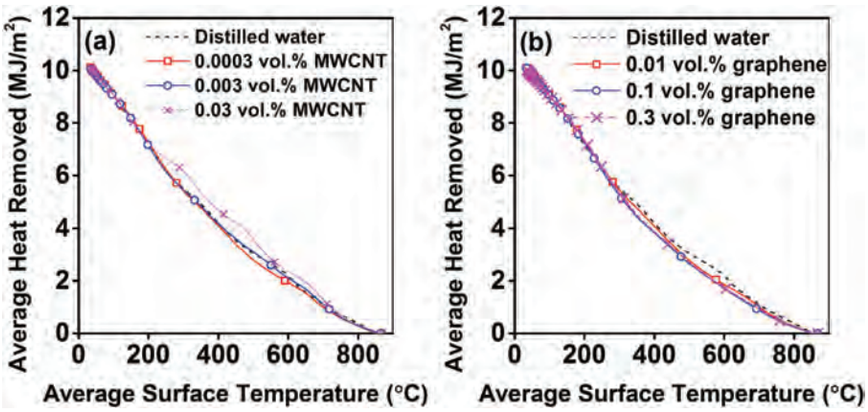

Fig. 22. Average heat removed versus average surface temperature during quenching with (a) MWCNT and (b) graphene nanofluids of various concentrations at impeller rotation rate of 1500 rpm.

quenching in nanofluids compared to water. This indicates higher hardness during quenching in nanofluids. To find an explanation to the increase in the cooling ability of nanofluids relative to water the thermophysical properties and contact angle of nanofluids were measured. Table III shows the thermophysical properties measured for distilled water and nanofluids. It shows that addition of nanoparticles of graphene and MWCNT did not cause any significant change in the viscosity, thermal conductivity and density of nanofluids compared to water. The thermal conductivity found of water and nanofluidsdetermined in the study, is in agreement with the benchmark study conducted by Buongiorno et al.[10] The measured surface tension of nanofluids were lower compared to water with the least surface tension obtained with 0.003 vol.% MWCNT and highest with water while the surface tension of other nanofluids had intermediate values.

To account for the increase in the cooling rates, boiling points of nanofluids were measured. It was found that MWCNT nanofluids had very much similar boiling points (99.5 °C) compared to distilled water. The boiling point of graphene nanofluids were lower only by a degree compared to that of water. To check for phase transformation of nanoparticles due to localised heating during quenching, the nanoparticles were heated upto 860 °C in a furnace and it was observed that they did not undergo any change in phase. Contact angle measurements obtained during spreading of a quench medium droplet on an Inconel substrate is shown in Figure 7.

The spreading curves for nanofluids clearly show reduced contact angle compared to nanofluids indicating that addition of nanoparticles to distilled water improved its wetting ability. Improved wetting of nanofluids on the surface of the metal is generally preferred as it aids in more uniform heat extraction compared to the liquids that do not exhibit good wetting.

The cooling curves recorded near the surface at various axial locations during quenching in water and nanofluids is shown in Figures 8 to 14. They show the dynamic nature of heat removal from the probe during quenching.

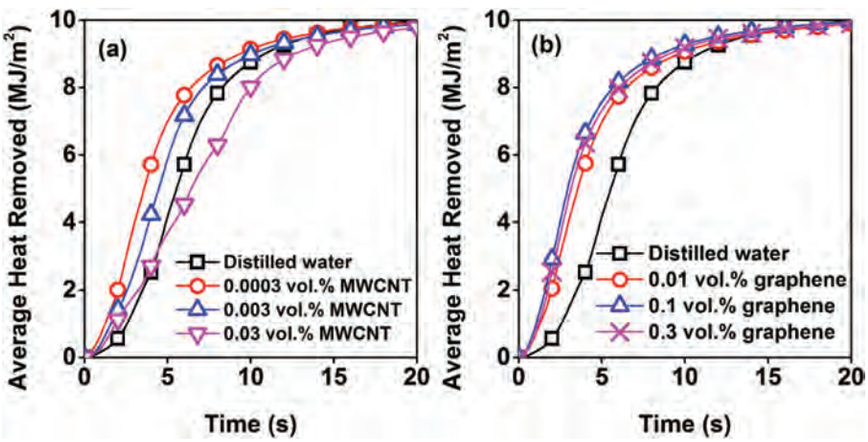

Fig. 23. Average heat removed versus time plot obtain during quenching with (a) MWCNT and (b) graphene nanofluids of various concentrations at impeller rotation rate of 1500 rpm.

The cooling curves show that the different locations of the probe are rewetted by the liquid medium at different times during quenching. Rewetting occurs when the vapor phase breaks causing the liquid quench medium to contact the probe. It is clearly seen that TC(4) thermocouple experiences shorter rewetting time compared to the other thermocouples. In other words, the location of the probe that comes first in contact with the liquid medium shows early heat loss compared to other locations. The difference in rewetting time observed at various axial locations

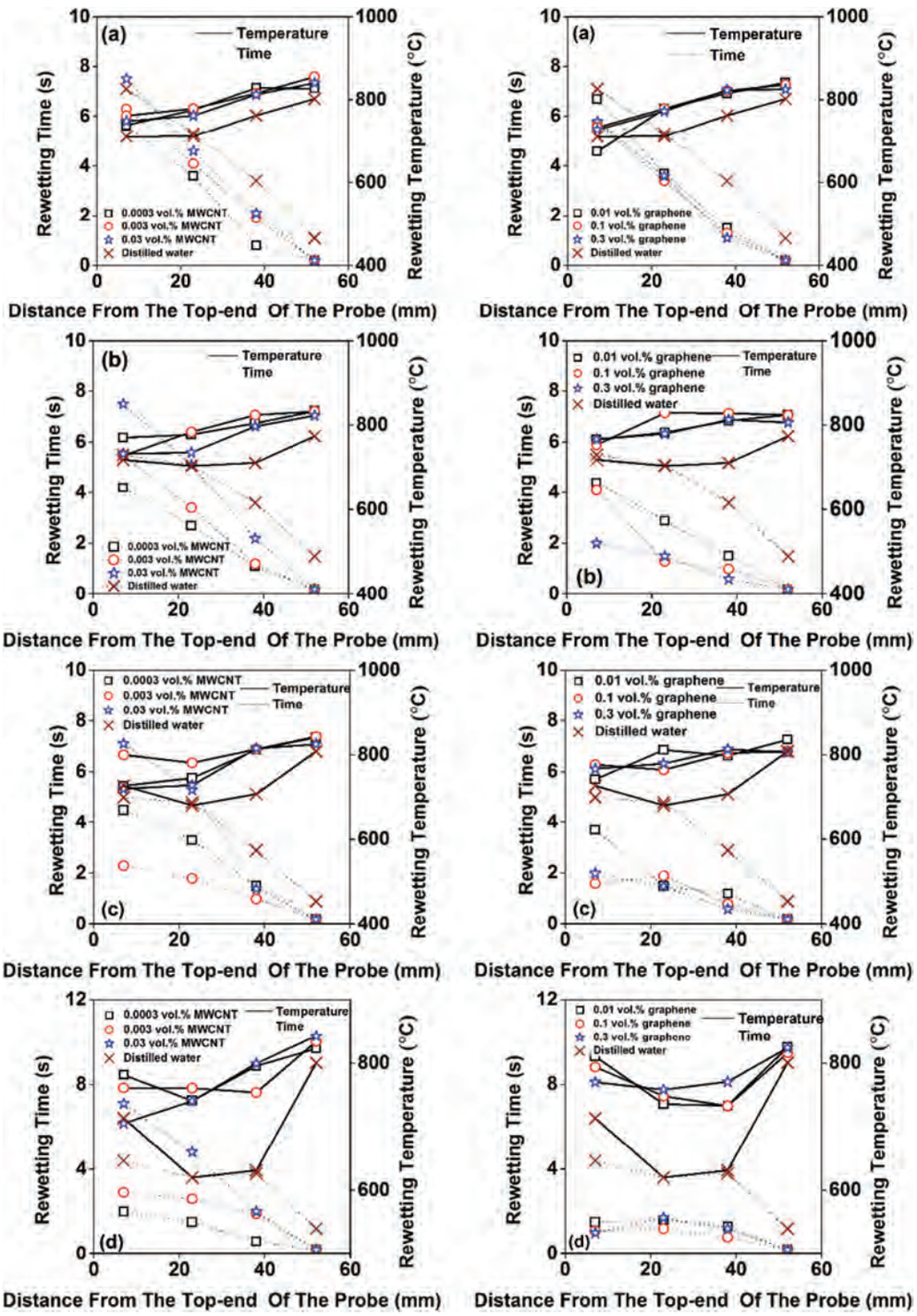

Fig. 24. Rewetting time and rewetting temperature obtained with water based graphene and MWCNT nanofluids of various concentrations under agitation rates of (a) still (b) 500 (c) 1000 and (d) 1500 rpm.

clearly indicates the formation, existence and progress of a rewetting front (formed by the loci of the boundary separating the vapour phase from the nucleate boiling phase). This rewetting front is responsible for differential cooling of the probe because it leads to simultaneous occurrence of vapor, nucleate boiling and convective cooling mechanisms of heat transfer on the probe surface. The cooling curves also show that faster cooling of the probe results with increase in the agitation rate of the quench medium.

The interfacial spatiotemporal heat flux estimated at various boundary heat flux segments during quenching in distilled water and nanofluids of MWCNT and graphene of various concentrations are shown in Figures 15 to 21.

The nature of these heat flux curves is similar to that of the cooling rate curves. The initial low value of heat flux was due to the insulating nature of the vapor phase that surrounded the probe. After this slow phase, the heat flux rises rapidly and reached a peak value due to the rapid heat removal by the nucleate boiling phase and then continues to reduce with slower removal of heat as the cooling progresses by convection cooling mechanism. The peak value of heat flux obtained under various agitation rate for the quench media are shown in Table IV. It shows that agitation of the liquid quench medium increased the rate of heat extracted from the probe. of the nanofluids, 0.01 vol.% graphene showed least average peak heat flux (2.58 MW/m^2) while the 0.1 vol.% graphene nanofluid had the highest average peak flux value (3.23 MW/m^2). The average peak heat flux values of other nanofluids showed intermediate values. The higher average peak heat flux value for nanofluids compared to water and is indicative of their higher and faster heat extraction capability.

Figure 22 shows the average heat removed by the nanofluids as a function of mean surface temperature at the agitation rate of 1500 rpm for water and nanofluids. These plots are obtained by integrating the heat flux curves. The average heat removed plots for MWCNT show that at dilute nanoparticle concentrations of 0.0003 and 0.003 vol.% the average heat removed by these nanofluids as a function of the average surface temperature is lower than that of water. At 0.03 vol.% concentration, MWCNT nanofluid shows more heat extraction with temperature compared to water. For the graphene nanofluids the heat removed with temperature were slightly below that of water at all the concentrations.

The lower average heat removed with average surface temperature was because of faster heat extraction by nanofluids compared to water and is shown in Figure 23. It clearly shows that heat extraction rates of graphene and MWCNT nanofluids of 0.0003 and 0.03 vol.% concentrations were faster compared with 0.03 vol.% MWCNT and distilled water and is attributed to enhanced Brownian motion of nanoparticles under agitated conditions.

The rewetting time and temperature obtained under various agitation conditions are shown in Figure 24. Rewetting time and temperature were obtained using the temperature data extracted at node locations on the surface of the axisymmetric meshed model of the probe corresponding to the nodes of the near surface thermocouples (used to measure temperature readings). These plots show that with increased agitation the time to rewet the probe was reduced and the rewetting temperatures were higher for nanofluids compared to water.

4. CONCLUSIONS

Nanofluids of graphene and MWCNT have lower wetting angles compared to water.

The surface tension of nanofluids were found to be lower than that of water with 0.003 vol.% MWCNT having the least surface tension of 48 mN/m.

Agitation rate of 1500 rpm caused a substantial reduction in the rewetting time for graphene nanofluids with 53% reduction in the rewetting time observed during quenching with 0.1 vol.% graphene nanofluid over that observed under still quench condition. The corresponding reduction during quenching with 0.0003 vol.% MWCNT nanofluid and water were about 28% and 8% respectively.

At 1500 rpm quenchant agitation, quenching of inconel in grapheme nanofluid of 0.1 vol.% concentration resulted in a mean peak heat flux of 3.23 MW/m^2 and was the highest obtained in this study. This was about 8% and 17% higher compared to the mean peak heat flux for 0.0003 vol% MWCNT and water respectively.

Viscosity, thermal conductivity and density of the quench media did not differ significantly. The increase in the heat flux during quenching with nanofluids under agitation was attributed to the enhanced Brownian motion of nanoparticles near the probe wall under turbulent conditions.

LIST OF SYMBOLS

CR_{max} — maximum cooling rate, °C/s
CR_{705} — cooling rate at 705 °C, °C/s
CR_{550} — cooling rate at 550 °C, °C/s
CR_{300} — cooling rate at 300 °C, °C/s
CR_{200} — cooling rate at 200 °C, °C/s
t_{A-B} — time at which vapor phase ends and nucleate boiling begins, *s*
T_{A-B} — temperature corresponding to t_{A-B}, °C
T_{max} — temperature at maximum cooling rate, °C
q — heat flux transients, MW/m^2.

References and Notes

1. H. J. French and T. E. Hamill, Publications of the National Bureau of Standards 1901 to June 1904, edited by U.S. Department of Commerce, RP103 (**1948**), pp. 399–418.
2. G. Ramesh and K. N. Prabhu, *Nanoscale Res. Lett.* 6, 15 (**2011**).
3. H. Kim, G. DeWitt, J. T. McKrell, and L.-W. Hu, *Int. J. Multiphase Flow* 35, 427 (**2009**).

4. D. Ciloglu and A. Bolukbasi, *Nucl. Eng. Des*. 241, 2519 (**2011**).
5. Z. Schauperl and S. Solic (eds.), Cooling characteristics of the water based nanofluids in quenching, *Proc. Int. Conf. MATRIB*, Vela Luka, Croatia, June–July (**2011**).
6. K. Babu and T. S. P. Kumar, *Int. J. Heat Mass Transfer*. 54, 106 (**2011**).
7. D. S. MacKenzie (eds.), Development of clay based nanofluids for quenching, *Proc. from 6th Int. Quenching Control distortion Conf. Incl. 4th Int. distortion Eng. Conf.*, Illinois, USA, September (**2012**).
8. M. Howson, B. P. Wynne, R. D. Mercado-Solis, L. A. Leduc-Lezama, J. Jonny, and S. Shaji, *J. Therm. Sci. Eng. Appl.* 8, 5 (**2016**).
9. T. S. Kumar, *Numer. Heat Transfer, Part B* 45, 541 (**2004**).
10. J. Buongiorno, D. C. Venerus, N. Prabhat, T. McKrell, J. Townsend, R. Christianson, Y. V. Tolmachev, P. Keblinski, L.-W. Hu, J. L. Alvarado, I. C. Bang, S. W. Bishnoi, M. Bonetti, F. Botz, A. Cecere, Y. Chang, G. Chen, H. Chen, S. J. Chung, M. K. Chyu, S. K. Das, R. D. Paola, Y. Ding, F. Dubois, G. Dzido, J. Eapen, W. Escher, D. Funfschilling, Q. Galand, J. Gao, P. E. Gharagozloo, K. E. Goodson, J. G. Gutierrez, H. Hong, M. Horton, K. S. Hwang, C. S. Iorio, S. P. Jang, A. B. Jarzebski, Y. Jiang, L. Jin, S. Kabelac, A. Kamath, M. A. Kedzierski, L. G. Kieng, C. Kim, J.-H. Kim, S. Kim, S. H. Lee, K. C. Leong, I. Manna, B. Michel, R. Ni, H. E. Patel, J. Philip, D. Poulikakos, C. Reynaud, R. Savino, P. K. Singh, P. Song, T. Sundararajan, E. Timofeeva, T. Tritcak, A. N. Turanov, S. V. Vaerenbergh, D. Wen, S. Witharana, C. Yang, W.-H. Yeh, X.-Z. Zhao, and S.-Q. Zhou, *J. Appl. Physics* 106, 9 (**2009**).